FAULT DETECTION IN A ROTATING SHAFT BY USING THE ELECTROMECHANICAL IMPEDANCE METHOD AND A TEMPERATURE COMPENSATION APPROACH

Aldemir Ap Cavalini Jr

aacjunior@mecanica.ufu.br

Denise Dias de Oliveira

denise@aero.ufu.br

Diogo de Souza Rabelo

diogo_rabelo@mecanica.ufu.br

Roberto Mendes Finzi Neto

finzi@mecanica.ufu.br

Valder Steffen Jr

vsteffen@mecanica.ufu.br

LMEst - Laboratory of Mechanics and Structures, Federal University of Uberlândia, School of Mechanical Engineering, Av. João Naves de Ávila, 2121, Uberlândia, MG, 38408-196, Brazil.

Abstract. *The aim of this paper relies on the correct detection of incipient faults in rotating shafts by using the so-called electromechanical impedance method. Basically, this structural health monitoring technique – SHM - monitors changes in the electric impedance of piezoelectric transducers bonded to (or embedded into) the host structure, through specific mathematic equations, the so-called damage metrics, to detect damage. This is possible once the electrical impedance of the transducer is directly related to the mechanical impedance of the structure. Previously, successful experimental tests were performed in a horizontal rotor supported by roller bearings in which PZT patches were bonded along the host structure. Although successful, the obtained results shown to be susceptible to changes in the environmental and machine temperatures. Aiming at overcoming the limitations faced, in this contribution a compensation technique is proposed. The variations on the measured impedance signatures are minimized by using a hybrid optimization method associated with different damage metrics.*

Keywords: *fault detection, electromechanical impedance method, temperature compensation, rotating shafts.*

1 INTRODUCTION

The detection of incipient cracks in shafts of rotating machines under operating condition is one of the most challenging problems in the field of rotordynamics. Visual examination, radiographic tests, ultrasonic tests, and dye penetrant inspection, are some examples of non-destructive techniques widely used for crack detection. These methods have proved to be costly, since satisfactory results rely on detailed and periodic inspections (Saavedra and Cuitiño, 2001). The techniques based on vibration measurements are recognized as promising SHM tools (Structural Health Monitoring). Thus, significant research effort has been directed in the recent years to crack detection, location, and severity estimation by using vibration signals (Doebling et al., 1998; Darpe et al., 2004; Cavalini Jr et al., 2014).

There are two widely accepted rules in industry for crack detection in rotating shafts. The first one is based on the monitoring of the synchronous vibration amplitude and phase. According to Bently and Hatch (2002), changes in the 1X amplitude and phase are the best primary indicator of crack presence. The second rule relies on the 2X vibrations, where the same authors state that if a cracked rotor has a steady unidirectional radial load, then a strong 2X response may appear when the rotor is turning at half of any balance resonance speed. Even using these principles, Bachschmid et al. (2010) reveal the great difficulty faced to detect a crack with 25% depth found in the shaft of a steam turbine that had been operating in this condition over 1 month at a constant speed. Therefore, currently, the attention of researchers is turning to more sophisticated methods that are able to identify incipient cracks (i.e. cracks that propagated by up to 25% of shaft diameter), which are usually hardly observable in the measured vibration signals.

Following a different approach, incipient damages were detected in a rotating shaft (17 mm diameter) by using the so-called electromechanical impedance method (Cavalini Jr et al., 2014). Through piezoelectric material sensor-actuators (PZT patches; 12 mm *x* 6 mm), the electromechanical impedance, which is directly related to the mechanical impedance of the rotor, was determined. Based on changes of the impedance signals damage could be detected (e.g., small mass addition and incipient cracks). In this case, rigid (and flat) PZT patches bonded on the shaft were used as sensor-actuators for the purpose of fault identification.

Although successful, the obtained results have shown to be susceptible to changes according to the environmental and machine temperatures. Aiming at overcoming these limitations, a temperature compensation technique is proposed in this work. The optimal effective frequency and amplitude shifts are determined from the solution of a typical inverse problem. The damage metric associated with two impedance signatures is minimized by using a hybrid optimization methodology. The evolutionary technique Differential Evolution (Storn and Price, 1995) is devoted to the global search. The heuristic optimizer is followed by the application of the direct method SQP (Sequential Quadratic Programming) to provide a successful local search (Vanderplaats, 2007). The proposed compensation technique is applied on the impedance signatures obtained from a horizontal rotating machine. Different structural conditions regarding the shaft of the rotor are evaluated in this contribution (Cavalini Jr et al., 2014).

It is worth mentioning that the temperature compensation methods are generally based on the effective frequency and amplitude shifts through correlation analysis. Sun et al. (1995) first proposed the use of cross-correlation between two impedance signatures to compensate for frequency shifts caused by temperature variation. Park et al. (1999) compensated for both the frequency and the magnitude shifts through a modified damage metric. Koo et al. (2009)

modified the method developed by Park et al. (1999) to develop effective frequency shift to compensate for temperature effects through maximization of the correlation coefficient. Despite a good agreement can be obtained by using those temperature compensation techniques, there are limitations regarding the frequency band. This is also true when the desired temperature range is extremely large, which could implicate poor matching in the signatures when the temperature gradient is very large (Rabelo, 2014).

2 IMPEDANCE BASED STRUCTURAL MONITORING

The impedance based SHM technique was first proposed by Liang et al. (1994). This technique uses small PZT patches (or MFC transducers) to monitor changes in the structure that may occur due to the appearing of damage (changes in stiffness, damping, and mass). When the PZT patch is bonded to the structure and a low electric voltage is applied, generally 1V (Raju, 1997), a strain is produced. Using a high excitation frequency (in terms of typical modal analysis testing), the dynamic response of the structure will represent only the behavior of the system in the local area around the sensor. The dynamic response of the induced mechanical vibrations is transmitted by the same PZT patch as an electrical signal. Thus, if an incipient damage appears in the system, changes can be observed in the electric response measured by the impedance sensors (dynamic response that leads to an impedance signature). The electromechanical model that quantifies and describes the measurement process is illustrated in Fig. 1 for a single degree of freedom system (mass *m*, stiffness *k*, and damping *c*; *V* and *I* are the voltage and current, respectively).

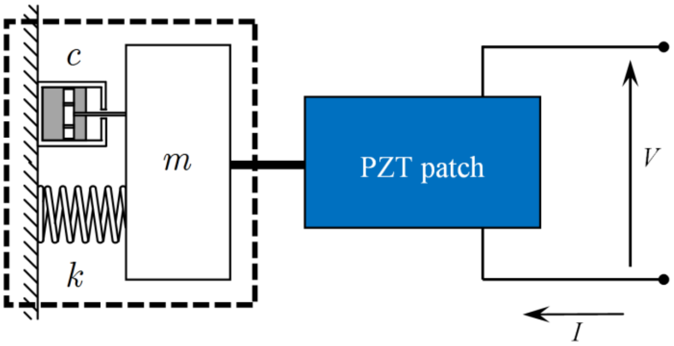

Figure 1. Electromechanical model that describes the process of measuring the impedance signature.

For this system, Liang et al. (1994) demonstrated that the admittance $Y_a(\omega)$ (inverse of the impedance) of the PZT patch can be written as a function of the combined PZT actuator and structure mechanical impedances, $Z_{ma}(\omega)$ and $Z_{me}(\omega)$, respectively, as given by Eq. (1):

$$Y_a(\omega) = I(\omega)\omega a\left\{\varepsilon_{33}^T\left[1 - I(\omega)\delta\right] - \frac{Z_{ma}(\omega)}{Z_{ma}(\omega) - Z_{me}(\omega)} d_{3x}^2 \hat{Y}_{xx}^E\right\} \tag{1}$$

where $\hat{Y}^E_{xx}$ is the complex Young's modulus of the PZT patch with zero electric field, d_{3x} is the piezoelectric coupling constant in the arbitrary *x* direction at zero electric field, ε^T_{33} is the dielectric constant at zero stress, δ is the dielectric loss tangent to the PZT patch, *a* is a geometric constant of the PZT patch, and is ω the frequency. Assuming that the mechanical properties of PZT patch do not vary over time used for monitoring, Eq. (1) shows that the electrical impedance of the PZT patch is directly related to the structure's impedance (damages cause changes in the structure's mechanical impedance).

Extensively applied in different structures, particularly in aircraft structures, the electromechanical impedance method operates at high frequencies (typically ranging from 30 kHz to 250 kHz, determined by a trial and error method) and has an accurate sensitivity to incipient damage (Inman et al., 2005). According to Park et al. (2003), for a simple PZT patch, a damage located at a distance up to 0.4 m can be identified in composite materials and up to 2 meters in bars consisting of a single metal. The impedance signature is determined by means an impedance analyzer. The structural integrity assessment is made based on the comparison of impedance signatures measured before and after the occurrence of a possible damage. A visual comparison is not enough, being necessary to use quantitative criteria. In this sense, the so-called damage metrics is defined, which is represented by scalar parameters that are able to represent numerically the difference between two measurements. Among the various damage metrics proposed, the root mean square (*RMS*), the deviation of the root mean square (*RMSD*), and the deviation of the correlation coefficient (*CCD*), are the mostly used.

As the first damage metric, Eq. (2) defines the root mean square (*RMS*).

$$RMS = \left\{ \sum_{i=1}^{n} \frac{\left[\mathrm{Re}\left(Z_{1i}\right) - \mathrm{Re}\left(Z_{2i}\right) \right]^2}{n} \right\}^{1/2} \tag{2}$$

where Re (Z_{1i}) is the real part of the impedance signature of the system without damage (reference value: *Baseline*) and Re (Z_{2i}) is the real part of the impedance signature of the system for an unknown structural condition, n is the number of points (frequency vector) of the impedance signal (i = 1, 2, ..., n).

The deviation of the root mean square (*RMSD*) is given by Eq. (3). This metric is not qualitatively affected when applied in impedance signatures obtained from different PZT patches (different amplitude levels).

$$RMSD = \left\{ \sum_{i=1}^{n} \frac{\left[\mathrm{Re}\left(Z_{1i}\right) - \mathrm{Re}\left(Z_{2i}\right) \right]^2}{\mathrm{Re}\left(Z_{1i}\right)^2} \right\}^{1/2} \tag{3}$$

The deviation of the correlation coefficient, *CCD*, is used to measure and interpret the information found in both data sets considered. The mathematical formulation of this metric is given by the difference between the first scale and the correlation coefficient *CC* of the signatures obtained from any measurement and its reference (Giurgiutiu and Zagrai, 2005). The greater the correlation coefficient, *CC*, the smaller will be the deviation *CCD* and smaller are the changes caused by the damage in the system.

$$CCD = 1 - CC = 1 - \frac{1}{n} \sum_{i=1}^{n} \frac{\left[\mathrm{Re}\left(Z_{1i}\right) - \mathrm{Re}\left(\bar{Z}_{1i}\right) \right] - \left[\mathrm{Re}\left(Z_{2i}\right) - \mathrm{Re}\left(\bar{Z}_{2i}\right) \right]}{S_{Z1} S_{Z2}} \tag{4}$$

where $Z_{1,i}$ is the impedance of the PZT patch measured at healthy conditions, $Z_{2,i}$ is the impedance for the comparison with the *baseline* measurement at frequency interval *i*. The symbols $\bar{Z}_{1i}$ and $\bar{Z}_{2i}$ represent mean values, while S_{Z1} and S_{Z2} represent standard deviations.

3 TEMPERATURE COMPENSATION

Figure 2 shows a flowchart to illustrate the proposed temperature compensation methodology. The method starts by obtaining the impedance signatures of the healthy analyzed system ($Imp_{baseline}$; temperature $T_{baseline}$). The impedance signatures of the system for an unknown condition ($Imp_{unknown}$; temperature $T_{unknown} \neq T_{baseline}$) are also required, so that the optimizer is responsible for shifting their effective frequency and amplitude. The $Imp_{unknown}$ signatures are compared with the $Imp_{baseline}$ ones by means of a given objective function, i.e., a damage metric, as presented by Eq. (2), Eq. (3), and Eq. (4) ($Imp_{baseline} = Z_1$ and $Imp_{unknown} = Z_2$). If the procedure converges to a minimum value of the objective function, the effects of temperature variation are compensated. If this is not the case, the optimization procedure will propose new effective frequency and amplitude shifts. The optimization process continues iteratively until convergence is assured, which can lead to temperature compensation (if the objective function is close to zero) or a damage indication associated with temperature compensation.

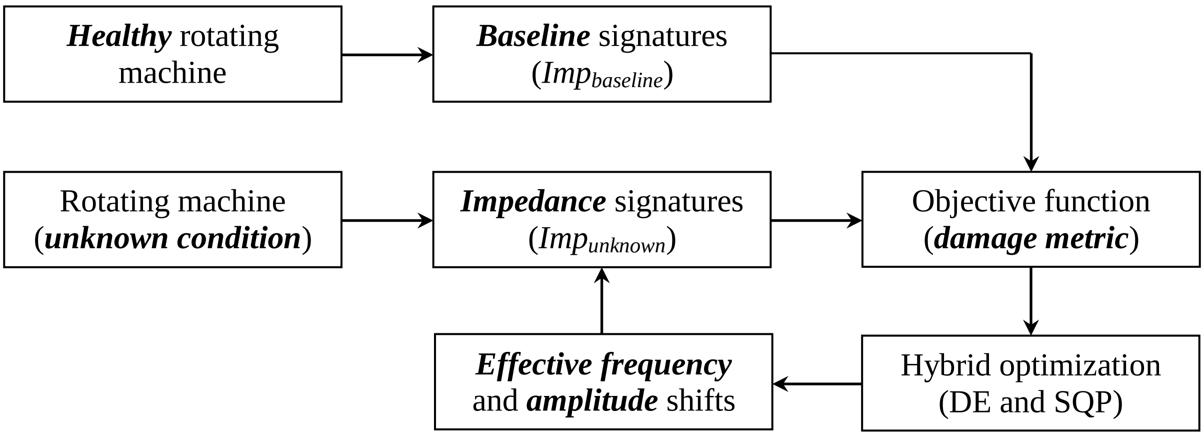

Figure 2. Temperature compensation flowchart.

In the present contribution, the proposed hybrid optimization technique is primarily devoted to minimize the influences of temperature variations during the impedance measurement process. However, the obtained results lead to the conclusion that different environmental or structure conditions can be compensated. The rotation speed, unbalance, pressure, and humidity, are some examples of operating conditions that may lead to changes in the impedance signatures, considering only case of healthy structure.

4 HYBRID OPTIMIZATION ALGORITHM

As mentioned, the proposed temperature compensation technique is based on the solution of a typical inverse problem, in which the optimal effective frequency and amplitude shifts are determined minimizing the damage metric associated with two impedance signatures. Therefore, the evolutionary technique Differential Evolution is devoted to the global search of the solution (i.e., the effective frequency and amplitude shifts). It is worth mentioning that the DE algorithm have to be performed n times to avoid local minima. The best result obtained by DE is used as starting point for the direct method SQP in order to obtain the local and refined solution.

The DE algorithm is an optimization technique that belongs to the family of evolutionary computation, which differs from other evolutionary algorithms in the mutation and recombination schemes. As previously mentioned, DE executes its mutation operation by adding a weighted difference vector between two individuals to a third individual. Then, the mutated individuals will perform discrete crossover and greedy selection with the corresponding individuals from the last generation to produce the offspring. The key control parameters for DE are the population size (NP), the crossover constant (CR), and the so-called weight (F). The pseudo-code of *DE* algorithm is presented in the Fig. 3, in which *P* is the population of the

Differential Evolution

Initialize and evaluate population P

while (not done) {

for (i = 0; $i < N$; i++) {

Create candidate $C_{[i]}$

Evaluate $C_{[i]}$

if ($C_{[i]}$ is better than $P_{[i]}$)

$P_{0[i]} = C_{[i]}$

else

$P_{0[i]} = P_{[i]}$}

$P = P_0$

}

Create candidate $C_{[i]}$

Randomly select parents $P_{[i1]}$, $P_{[i2]}$, and $P_{[i3]}$

where i, i_1, i_2, and i_3 are different.

Create initial candidate

$C'_{[i]} = P_{[i1]} + F \times (P_{[i2]} - P_{[i3]})$.

Create final candidate $C_{[i]}$ by crossing over the genes of $P_{[i]}$ and $C'_{[i]}$ as follows:

for (j = 0; $j < N$; j++) {

if ($r < CR$)

$C_{[i][j]} = C'_{[i][j]}$

else

$C_{[i][j]} = P_{[i][j]}$

}

Figure 3. The pseudo-code of *DE* algorithm.

current generation, and *P'* is the population to be constructed for the next generation, $C_{[i]}$ is the candidate solution with population index i, $C_{[i][j]}$ is the j-th entry in the solution vector of $C_{[i]}$, and r is a random number between 0 and 1.

Storn and Price (1995) have given some simple rules for choosing the key parameters of DE for general applications. Normally, *NP* should be about 5 to 10 times the dimension of the problem (i.e., number of design variables). As for F, it lies in the range between 0.4 and 1.0. Initially, $F = 0.5$ can be tried, and then F and/or *NP* can be increased if the population converges prematurely. Storn et al. (2005) proposed various mutation schemes for the generation of new candidate solutions by combining the vectors that are randomly chosen from the current population. In the applications of this paper, the *rand* / 1 scheme was used.

According to Vanderplaats (2007), the SQP algorithm is a direct method used for dealing with constrained minimization problems in which the search direction S is found by solving a sub problem with a quadratic objective and linear constrains. For this aim, it is determined by creating a quadratic approximation of the augmented objective function (i.e., from the association of the Lagrange multipliers λ with an exterior penalty technique) and a linear approximation for constrains, as shows Eq. (5).

$$\begin{aligned} &\text{Minimize:} \quad Q(S) = F(X) + \nabla F(X)^T S + \frac{1}{2} S^T B S \\ &\text{Subject to:} \quad \nabla g_j(X)^T S + \delta_j g_j(X) \leq 0 \quad j = 1, m \\ &\qquad\qquad\quad \nabla h_k(X)^T S + \bar{\delta} h_k(X) \leq 0 \quad k = 1, l \end{aligned} \tag{5}$$

where X is the vector of design variables and B is initially an identity matrix that will be updated on subsequent iterations. The parameters δ_j and $\bar{\delta}$ are used to prevent inconsistences between the linearized constrains g_j and h_k (i.e., typically $0.9 \leq \bar{\delta} \leq 0.95$). The δ_j parameter is defined as follows:

$$\begin{aligned} &\delta_j = 1 \quad if \;\; g_j(X) < 0 \\ &\delta_j = \bar{\delta} \quad if \;\; g_j(X) \geq 0 \end{aligned} \tag{6}$$

The direction-finding problem described by Eq. (5) is actually a quadratic programming problem and special techniques should be used for its solution. The associated one-dimensional search is written from the determined search direction S and an exterior penalty function ϕ, as given by Eq. (7).

$$\phi = F(X) + \sum_{j=1}^{m} u_j \{\max[0, g_j(X)]\} + \sum_{k=1}^{l} u_{m+k} \left| h_k(X) \right| \tag{7}$$

where $X = X^{q-1} + \alpha_p S$, $u_j = |\lambda_j|$ (j = 1, $m + l$) in the first iteration, $u_j = \max[|\lambda_j|, 0.5 (u'_j + |\lambda_j|)]$ for the subsequent iterations, and $u'_j = u_j$ from the previous iteration. In this case, $\alpha_p = 1$.

5 EXPERIMENTAL APPLICATION

Figure 4 shows the test rig used in the application of the SHM technique proposed by this work, i.e., the detection of incipient transverse cracks in rotating shafts by using the electro-mechanical impedance method. This machine is composed by a flexible steel shaft with 860 mm length and 17 mm diameter, and two rigid discs, both of steel with 150 mm diameter and 20 mm thickness (approximately 2.65 kg each). The shaft is supported by two ball bearings. The system is driven by a DC electric motor of 0.5 CV (*Varimot*® model BN90M). The interaction between the electric motor and the shaft is minimized by means of a special coupling named *Lami-Torq* (*Acoplast*® model GTG 402 100). From a representative mathematical model of the rotor (finite element model), the first two critical speeds were determined, being approximately: 1685 rev/min (28.1 Hz) and 5430 rev/min (90.5 Hz).

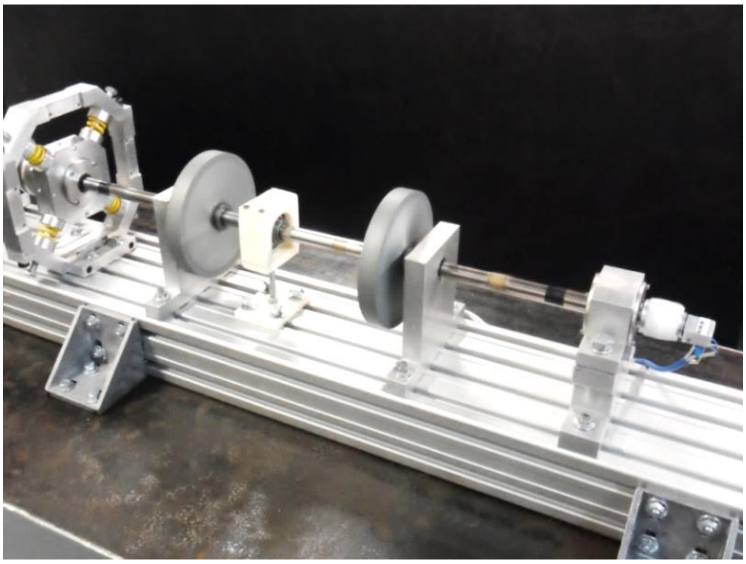

Figure 4. Test rig used in the application of the electromechanical impedance method.

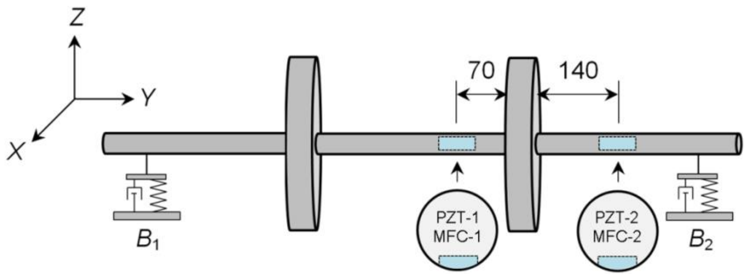

Figure 5. Distribution of the PZT patches along the shaft and on the face of the disc (dimension in mm).

In this application, two PZT patches (12 *x* 3 mm) and two MFCs (*Macro Fiber Composite*) were distributed along the shaft in two measurement planes to cover the largest possible surface for detection (i.e., 01 PZT patch, 01 MFC, and 01 thermocouple considered in each measurement plane; see Fig. 6). Fig. 5 shows a schematic arrangement with each of the four transducers bonded to the system, namely PZT-1, MFC-1, PZT-2, and MFC-2 (numbered starting from the hybrid bearing; B_1 in Fig. 4).

Figure 6 shows the rigid PZT patch (left hand side; Sparkler® model SP4), the flexible transducer used here (right hand side; Smart Material® model M0714-P2), and the thermocouple used in this application. Both transducers were bonding on the shaft by using the glue Rysol®, selected for its good adhesion (piezoelectric patches *versus* steel structures). Regular glue was used to bond the thermocouple on the shaft surface.

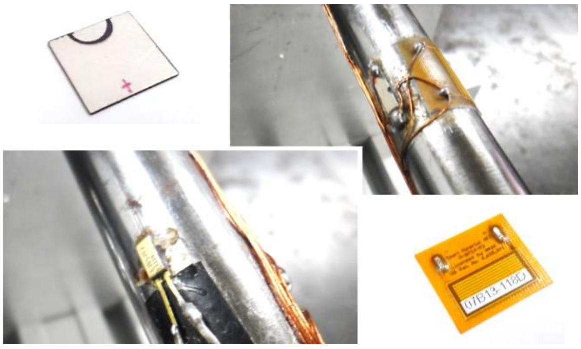

Figure 6. PZT patch and the MFC transducer (flexible actuator) used in this application.

For the measurement of the impedance signatures of the transducers (and the temperature) with the test rig under operation condition (sending excitation signals to the transducers and acquiring the responses), a slip ring was used (*MOOG*® model EC3848-10). This device is able to transfer electrical signals from fixed to rotating parts (and vice-versa) with low noise interference, even with the rotor operating at high speeds (according to the manufactures, the device is able to transfer electrical signals from accelerometers with the rotor operating in a range of 0 to 10000 rev/min).

Using a low-cost impedance measurement system (Finzi Neto et al., 2011), with the rotor at rest, a frequency sweep was applied to each transducer in the range between 0 and 200 kHz for determining the damage sensitive regions in the impedance signature. The results obtained from MFC-2 were discarded because this sensor presented incoherent results during the tests. Table 1 shows the frequency bandwidths determined. Note that the bands are delimited at high frequencies, which, as previously mentioned, allows for detecting incipient damage.

Table 1. Frequency bandwidths used for the transducers used.

	Frequency bandwidth (kHz)	
Transducer	From	To
PZT-1	101.00	109.00
MFC-1	167.75	169.75
PZT-2	166.00	174.00

The tests with the proposed methodology included the analysis of two structural conditions. In the first one (StrCnd-1), the bearing wear used in a loading device for crack initiation localized at approximately 70 mm from one of the discs. It is worth mentioning that the ball bearing used by the loading device (Fig. 7) had not worked before this application. The impedance signatures are sensitive to incipient structure modifications (e.g., incipient wear of ball bearings). Therefore, this structural modification was evaluated in order to avoid a false indication of damage in further applications of the proposed SHM technique.

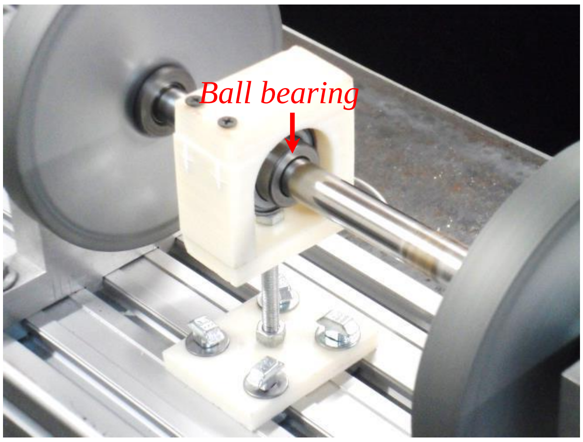

Figure 7. Loading device for crack nucleation (StrCnd-1).

The second analysis of the rotor condition (StrCnd-2) is a destructive damage. In this case, a notch was performed along the shaft cross-section. This was done about 140 mm from one of the discs (70 mm from PZT-1 and MFC-1; region delimited by the discs). The machining work leaded in a notch of approximately 2.5 mm depth (about 15% over the shaft diameter), as shown in Fig. 8.

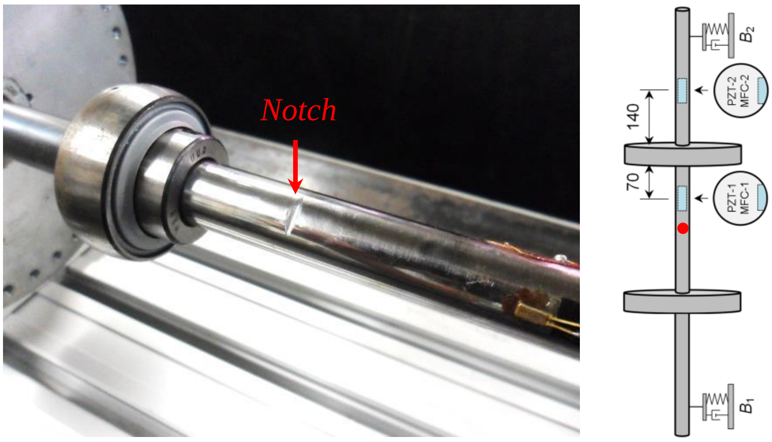

Figure 8. Details of the notch performed on the shaft surface (StrCnd-2).

In the analysis of both presented structural conditions, the rotor was kept operating under 800 rpm (balanced rotor; balancing performed by using the method of the four runs without phase). Different operating speeds and unbalance conditions were evaluated, leading to similar results (not presented here). The impedance signals were calculated from an average of 10000 measurements (impedance signatures with 1000 frequency points). This high number of measurements actually reduces the incidence of noise that arises from the dynamic behavior of the rotor (together with some electrical effects). Additionally, 80 measurements were performed for each structural condition (i.e., pristine, StrCnd-1, and StrCnd-2 rotor conditions). The analysis of the StrCnd-1 condition was repeated 2 times, leading to 160 measurements. In all tests, the temperature of the rotating system was controlled in the range between 20^0C to 24^0C.

Temperature variation plays a major role when a structure is being monitored with PZT patches. The effect of the temperature variation is presented in Fig. 9 to illustrate the capability of the compensation techniques when the temperature gradient is large. The main effects of temperature can be stated as horizontal and vertical shifts, as can be seen in Fig. 9b as well as changes in some of the peak amplitudes. Fig. 9a shows an aluminum plate of dimensions 305 *x* 305 *x* 3 mm, instrumented with a PZT patch type 5H with 15 mm diameter *x* 1 mm thickness attached on a central position. The tests were performed inside the environmental chamber ESPEC model EPL-4H, whose temperature resolution is of 0.5ºC after 30 minutes of settling time to stabilize the internal temperature. The temperature range utilized was from 0ºC to 50ºC in steps of 10ºC. Each impedance signature was measured with 600 points and the frequency range was from 63 kHz to 66 kHz. By analyzing Fig. 9b, the effects of the temperature can be seen predominantly as horizontal shifts due to changes in the resonance frequencies of the system. Vertical shifts can also be seen due to the change in the capacitance of the sensor, as well as changes in some peak amplitudes. Fig. 9c shows the results obtained with the compensation temperature technique proposed by Rabelo (2014). In this case, only one *baseline* was recorded at -30ºC, and each signature was measured with 600 data points, after 30 minutes of settling time for temperature stabilization. Overall, it can be observed that the temperature compensation procedure provides good agreement for the impedance signatures in a wide temperature range. However, since there is some variation in peak amplitudes, a perfect match in practical application will rarely occur, as demonstrated by the resonance peak close to 64 kHz in Fig. 9c. Despite a good agreement can be obtained with the temperature compensation techniques, there are limitations regarding the frequency band. This is also true when the desired temperature range is extremely large, which could implicate poor matching in the signatures when the temperature gradient is very large.

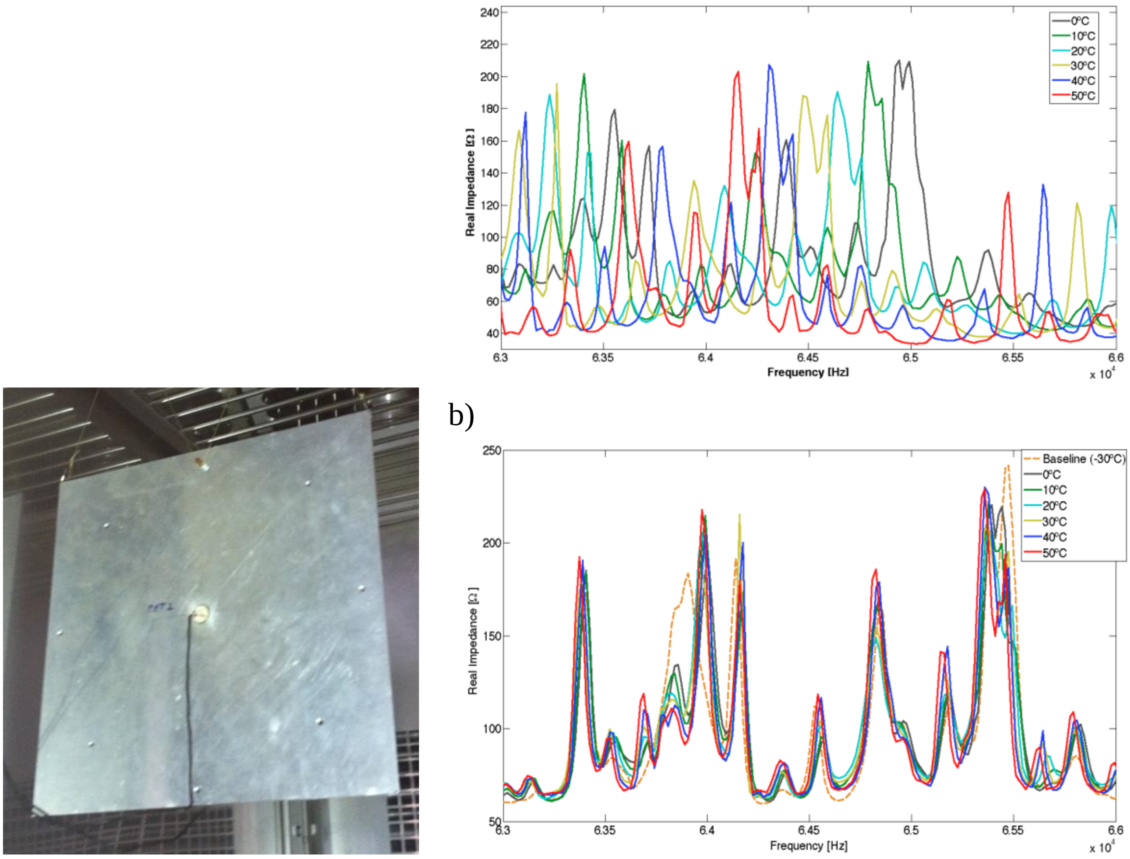

Figure 9. Temperature variation effects on impedance signatures: a) instrumented Al plate; b) impedance signals shifted with temperature changes; c) impedance signatures with compensation.

Regarding the proposed temperature compensation technique, the evolutionary minimization process was performed 5 times, considering 10 individuals in the initial population of the DE algorithm. As mentioned, the direct algorithm SQP was associated with the DE technique in order to improve the search process.

Figure 10a shows the non-compensated and compensated *RMS* values (Eq. (2)) obtained by using PZT-1 and considering the three analyzed structural conditions. The associated impedance signatures are presented by Fig. 10b, in which the black curves indicates the measures obtained after the application of the proposed compensation technique. Note that the undesirable effects provided by the temperature variation on the measured impedance signatures were minimized with the compensation process (see Fig. 10a and Fig. 10b). Additionally, it can be observed in Fig. 10c that the PZT-1 was able to detect only the notch performed along the shaft cross-section (i.e., structural condition StrCnd-2).

Figure 11 and Figure 12 show the non-compensated and compensated *RMS* values obtained by using MFC-1 and PZT-2, respectively, considering the three analyzed structural conditions. Note that the undesirable effects provided by the temperature variation on the measured impedance signatures were minimized with the compensation process considering both transducers (as well as verified in the results presented by Fig. 10). Additionally, it can be observed that MFC-1 and PZT-2 were able to detect successfully both StrCnd-1 and StrCnd-2 structural conditions (see Fig. 11c and Fig. 12c, respectively). This leads to the conclusion that there is a difference involving the electromechanical coupling of these

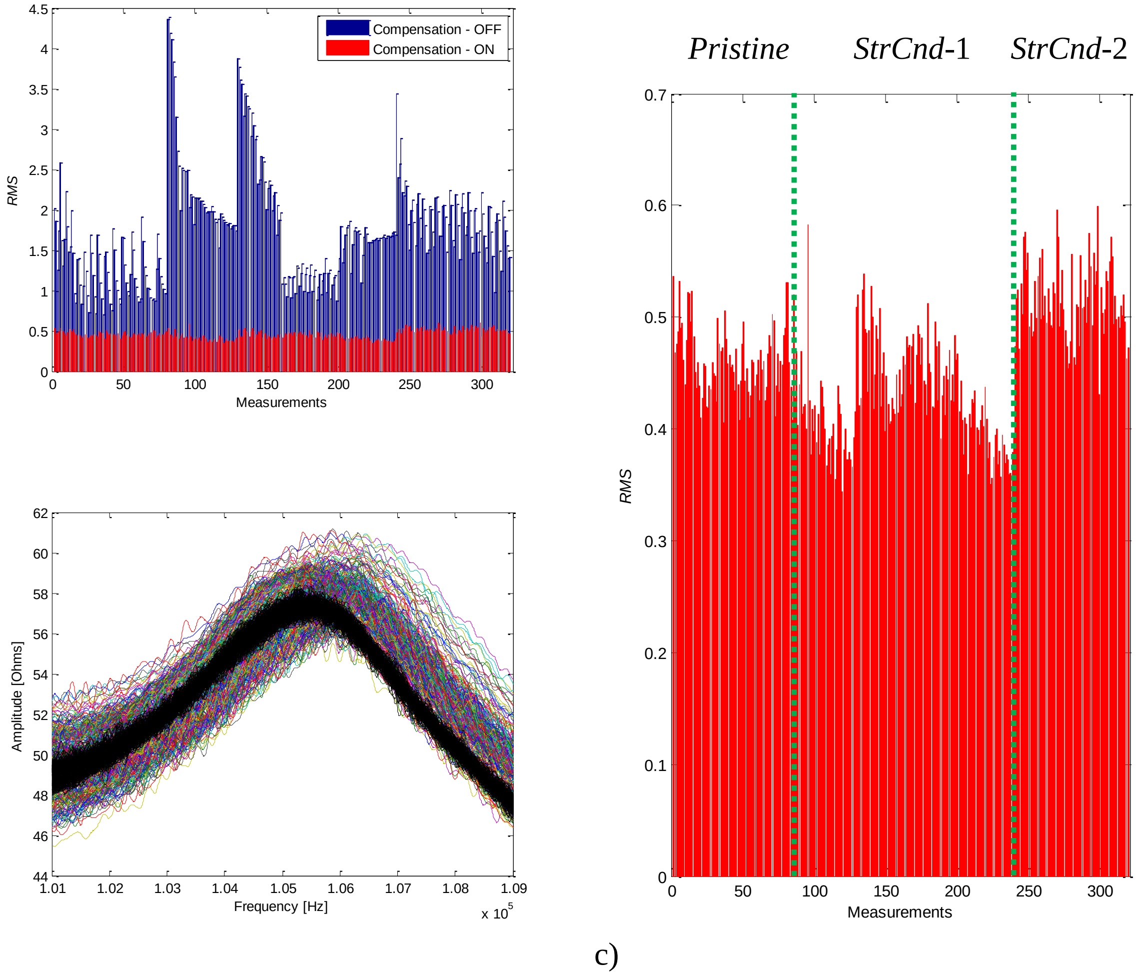

Figure 10. Non-compensated and compensated *RMS* values obtained by using PZT-1 and considering the three analyzed structural conditions

transducers with the shaft (probably due to the glue adhesion). Note that the PZT-2 is further from the considered “damages” than the PZT-1 (and MFC-1; see Fig. 4 and Fig. 5). The temperature compensation technique was also applied on the measured impedance signatures by using the *RMSD* damage metric (Eq. (3)) as objective function. However, the results were similar to those obtained by using the *RMS* damage metric (Eq. (2)).

Figure 13a shows the non-compensated and compensated *CCD* values (Eq. (4)) obtained by using PZT-1 and considering the three analyzed structural conditions. The associated impedance signatures are presented by Fig. 13b, in which the black curves indicates the measures obtained after the application of the proposed compensation technique. The results obtained by using MFC-1 and PZT-2 are shown in Fig. 14 and Fig. 15, respectively. Note that the proposed technique was not able to minimize the temperature effects considering the *CCD* damage metric as objective function. It can be observed that only the variation verified on the effective frequency shift of the impedance signatures was mitigated, as demonstrated by Fig. 13b, Fig. 14b, and Fig. 15b. Therefore, the *CCD* damage metric seems to be more sensitive to the frequency shift.

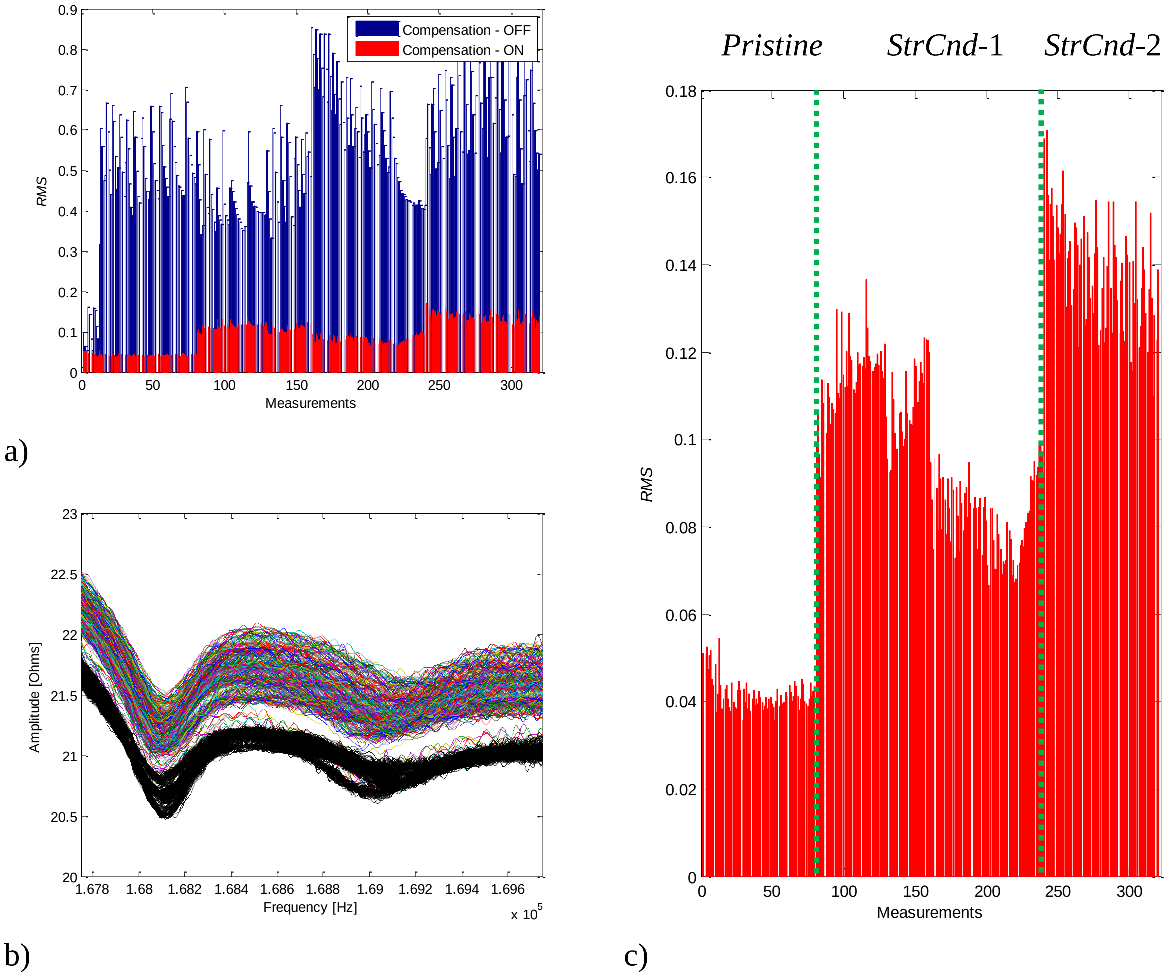

Figure 11. Non-compensated and compensated *RMS* values obtained by using MFC-1 and considering the three analyzed structural conditions

6 CONCLUSION

The results shown in the present contribution demonstrate the efficiency of the electromechanical impedance method associated with a temperature compensation technique for the detection faults in rotating shafts. As seen, the proposed SHM technique was evaluated for the rotor under operation, leading to satisfactory results. The rotordynamic applications were made possible by the use of a special device, the slip ring. The high frequency band is an advantage of the method since it permits the detection of damages even the ones far from the transducer (PZT patch or MFC). In this contribution, the variations on the measured impedance signatures due to the temperature effects were minimized by using a hybrid optimization method. Three damage metrics were used as objective function of the associated minimization problem, namely *RMS*, *RMSD*, and *CCD*, in which only the two first were able to mitigate the influence of the temperature on the measured impedance signatures (providing similar results). It was observed that only the variation verified on the effective frequency shift of the impedance signatures was minimized when the *CCD* damage metric was used as objective function. Further studies will encompass evaluations of different compensation techniques for comparison purposes.

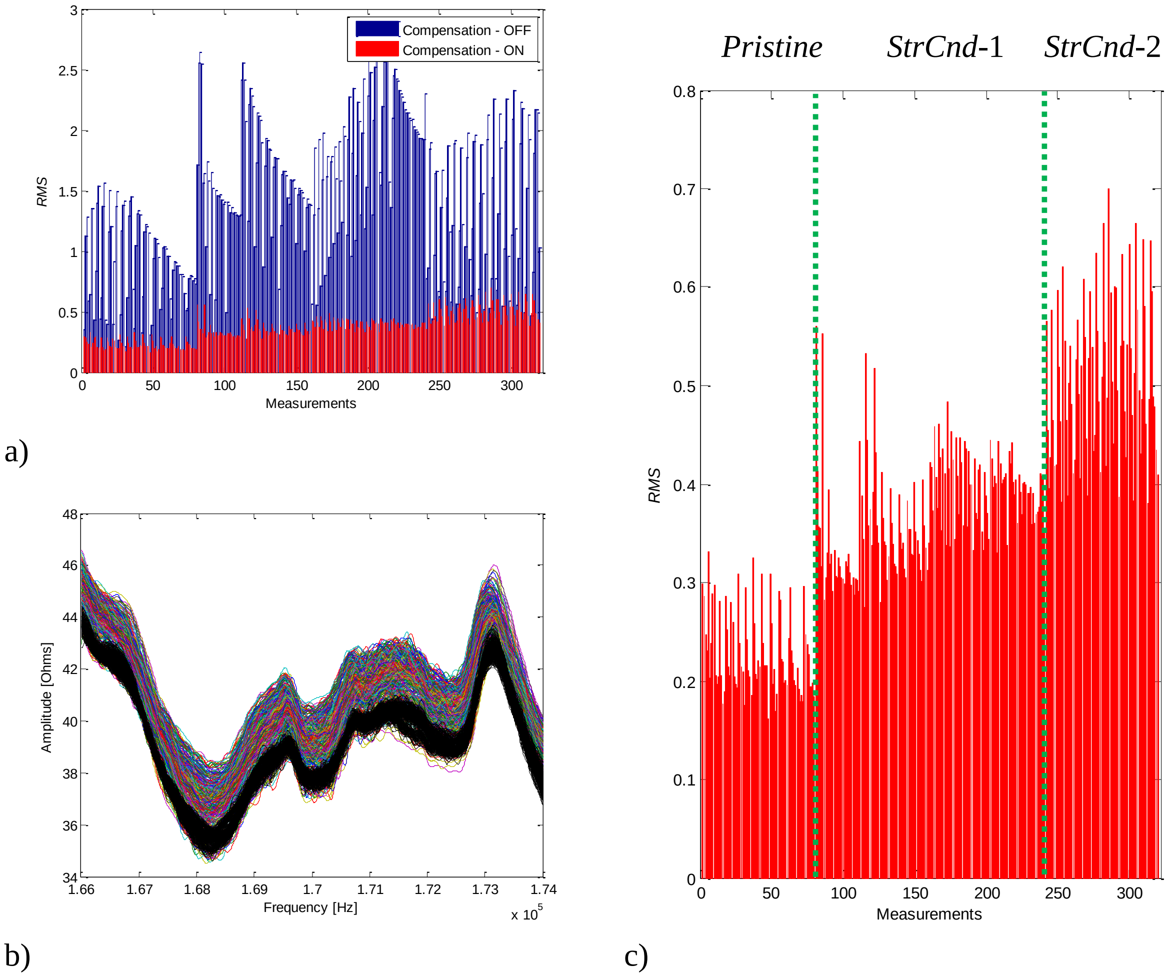

Figure 12. Non-compensated and compensated *RMS* values obtained by using PZT-2 and considering the three analyzed structural conditions

ACKNOWLEDGEMENTS

The authors are thankful to the Brazilian Research Agencies FAPEMIG and CNPq (INCT-EIE) and also to CAPES for the financial support provided for this research effort.

REFERENCES

Bachschmid, N., Pennacchi, P., Tanzi, E., 2010. *Cracked rotors: a survey on static and dynamic behaviour including modelling and diagnosis*, Springer.Bently, D. E., Hatch, C. T., 2002. *Fundamentals of rotating machinery diagnostics*. Bently Pressurized Bearing Company, Minden, NV, USA.

Cavalini Jr, A. A., Finzi Neto, R. M., Steffen Jr, V., 2014. Impedance-based fault detection methodology for rotating machines. *Structural Health monitoring*, vol. 1, n. 1, pp. 1-13.

Darpe, A. K., Gupta, K., Chawla, A., 2004. Coupled bending, longitudinal and torsional vibrations of a cracked rotor. *Journal of Sound and Vibration*, vol. 269, n. 1, pp. 33-60.

Doebling, S. W., Farrar, C. R., Prime, M. B., 1998. A summary review of vibration-based damage identification methods. *Shock and Vibration Digest*, vol. 30, n. 2, pp. 91-105.

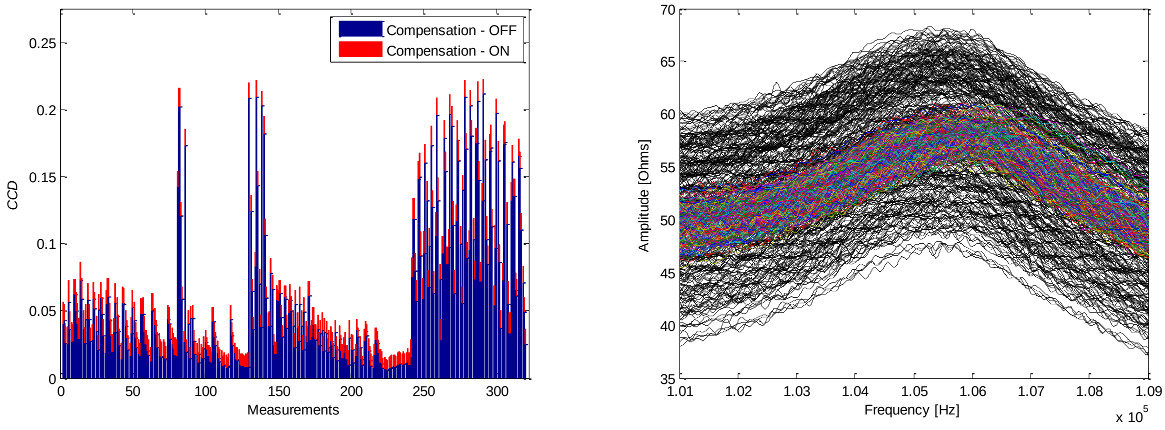

a) b)

Figure 13. Non-compensated and compensated *CCD* values obtained by using PZT-1 and considering the three analyzed structural conditions

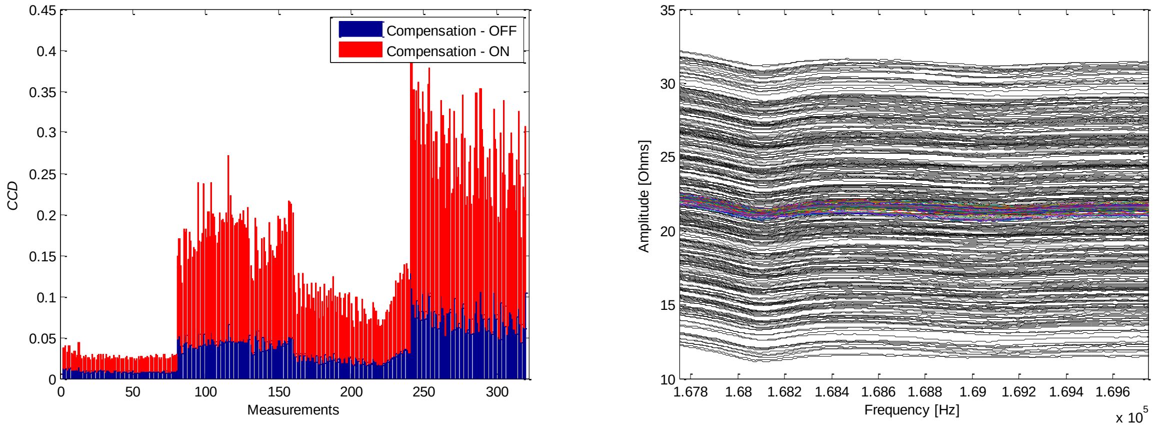

a) b)

Figure 14. Non-compensated and compensated *CCD* values obtained by using MFC-1 and considering the three analyzed structural conditions

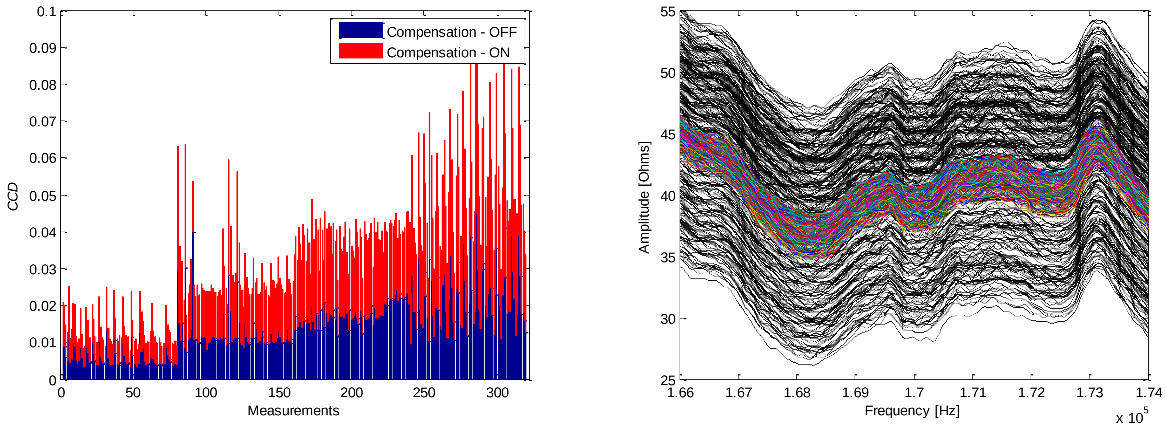

a) b)

Figure 15. Non-compensated and compensated *CCD* values obtained by using PZT-2 and considering the three analyzed structural conditions

Finzi Neto, R. M., Steffen Jr, V., Rade, D. A., Gallo, C. A., Palomino, L. V., 2011. A low-cost electromechanical impedance-based SHM architecture for multiplexed piezoceramic actuators. *Structural Health Monitoring*, vol. 10, n. 4, pp. 391-402.

Giurgiutiu, V., Zagrai, A., 2005. Damage detection in thin plates and aerospace structure with the electro-mechanical impedance method. *Structural Health Monitoring*, vol. 4, n. 2, pp. 99-118.

Inman, D. J., Farrar, C. R., Lopes Jr, V, Steffen Jr, V., 2005. *Damage prognosis: for aerospace, civil and mechanical systems*, Wiley.

Koo, K. Y., Park, S., Lee, J. J., Yun, C. B., 2009. Automated impedance-based structural health monitoring incorporating effective frequency shift for compensating temperature effects. *Journal of Intelligent Materials Systems and Structures*, vol. 20, n. 4, pp. 367-377.

Liang, C., Sun, F. P., Rogers, C. A., 1994. Coupled electromechanical analysis of adaptive material systems: determination of the actuator power consumption and system energy transfer. *Journal of Intelligent Material Systems and Structures*, vol. 5, pp. 12-20.

Park, G., Kabeya, K., Cudney, H. H., Inman, D. J., 1999. Impedance-based structural health monitoring for temperature varying applications. *JSME International Journal*, vol. 42, n. 2, pp. 249-258.

Park, G., Sohn, H., Farrar, C. R., Inman, D. J., 2003. Overview of piezoelectric impedance-based health monitoring and path forward. *The Shock and Vibration Digest*, vol. 35, n. 6, pp. 451-463.

Rabelo, D. S., 2014. *Impedance-based structural health monitoring incorporating compensation of the temperature variation effect*. M.S. dissertation, Federal University of Uberlandia, Brazil.

Raju, V., 1997. *Implementing impedance-based health monitoring*. PhD Thesis, Virginia Polytechnic Institute and State University, Virginia.

Saavedra, P. N., Cuitiño, L. A., 2002. Vibration analysis of rotor crack identification. *Journal of Vibration and Control*, vol. 8, pp. 51-57.

Storn, R., Price, K., 1995. Differential evolution: a simple and efficient adaptive scheme for global optimization over continuous spaces. *International Computer Science Institute*, vol. 12, n. 1, pp. 1-16.

Storn, R. M., Price, K. V., Lampinen, J. A., 2005. *Differential evolution - a practical approach to global optimization*, Springer, Natural Computing Series.

Sun, F. P., Chaudhry, Z., Liang, C., Rogers, C.A., 1995, Truss structure integrity identification using PZT sensor-actuator. *Journal of Intelligent Materials Systems and Structures*, vol. 6, n. 1, pp. 134-139.

Vanderplaats, G. N., 2007. *Multidiscipline design optimization*, Vanderplaats Research & Development.